HELIOSTAT FIELD EFFICIENCY TEST OF BEAM DOWN CSP PILOT PLANT EXPEREMINATAL RESULTS

Marwan Mokhtar[1], Irene Rubalcaba[1], Steven Meyers[1], Abdul Qadir[1], Peter Armstrong[1], Matteo Chiesa[1]

Masdar Institute of Science and Technology, Laboratory of Energy and Nano-Science (LENS), Abu Dhabi, UAE.

Phone: +971 698 8122; fax: +971 2 698 8121; e-mail: mmokhtar@masdar.ac.ae

Abstract

A test for studying the performance of individual heliostats of the beam down pilot plant was performed. The goal of this test is to get better understanding of the features as well as the issues associated with the unique heliostats used in this plant. The method for comparing the flux distribution maps is first presented; this method is meant for analyzing a large amount of data automatically and without having to inspect each flux map individually. Three parameters where chosen to assess each flux map, they are a measure of 1) overall DNI resource utilization 2) concentration quality of the heliostat and 3) centering of the flux map. This method is then applied to the experimental data obtained by testing the heliostat field for six days and a summary of the results is presented at the end.

I. Introduction

In central receiver plants the heliostat field layout is of exceptional importance. A considerable portion of the total losses in tower plants are due to cosine losses, blocking and shading. These are mainly associated with the heliostat field layout. Heliostat field layout is a topic which has been investigated over the years e.g. [1],[2]. However, simulation studies are not often validated because validation data is hard to come by. Moreover the practical limits of mirror alignment and shape fidelity, which in turn determine optical performance, can only be learned from field measurements. In this paper we present experimental data from performance tests of the heliostat field of a 100 kW_{th} beam down pilot plant in Masdar City [3]. The heliostat field is shown in Figure 1. The field consists of 33 ganged-type heliostats of 8.5 m^2 each as shown in Figure 1 right. Heliostats are arranged in three main fields (sectors) of equal size, North, East and West. Although it is common practice to have only a North field in such a small plant, a surrounding field was chosen for test purposes.

A test for studying the performance of individual heliostats was performed; this test helps us to better understand the unique aspects as well as the problems associated with the unusual heliostats used in this pilot plant in addition to the plant's unique optical design. The data will also useful in later stages for developing and verifying a model of the plant.

Figure 1Beam Down 100 kWth heliostat field layout.

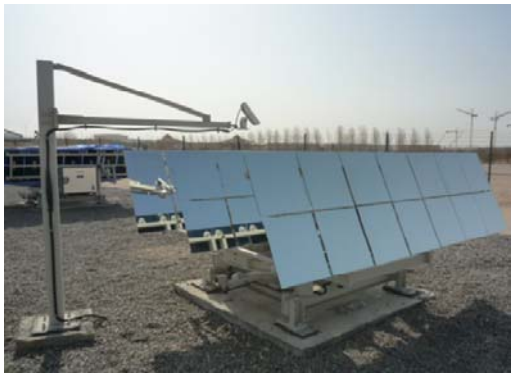

Figure 2 Typical ganged type heliostat and tracking sensor. The sensor arm and heliostat azimuth axis are aligned on a common radial line extending from the tower axis, which is to the left.

II. Brief on the Experimental Setup

The experimental setup in the beam down pilot plant consists of a CCD imaging device (2D Color Analyzer from Konica Minolta, Model:CA2000) which provides high-resolution two-dimensional measurement of the luminance distribution on the receiver plane. The CCD device is placed in the center of the secondary reflector allowing it to take images of the flux distribution of the entire receiver during operation. The receiving plane is made of white ceramic tiles which approximate a Lambertian target. Eight heat flux sensors are placed on the receiver in order to take point measurement of the radiation incident on the target and are used to calibrate the CCD images. These sensors are not used in this test.

III. Method of Comparing Heliostat Flux Distribution Maps

There are two important features of a flux distribution map which are of interest, one is the total energy sum and the other is the distribution of the flux on the receiving plane, the later includes two more parameters of interest, centering and concentration.

By centering we mean the deviation of the centroid of a certain flux map from the geometrical center of the target (see Figure 3), this is mainly a result of errors in aligning the secondary reflector mirrors or/and the tracking photo-sensor of the heliostats, centering is a problem that could be easily resolved relative to other problems, thus we will isolate it by basing all our analysis of the flux maps on their centroid rather than the geometrical center. The (offset) between the geometrical center and the centroid of the flux map will be used as a measure of centering error.

To facilitate the comparison of flux distribution maps of all the heliostats in a field, it is advantageous to combine the other two important merits into one quantity (total energy and concentration). Problem heliostats can then be identified for further visual and statistical inspection of individual flux density maps or for other more detailed studies.

Figure 3 illustrates a typical flux density map of (980x980) pixels, the area of interest to us is a square within the 980 x 980 pixel region of approximately 700 x 700 pixel which corresponds to the 4m x 4m target. Thus a pixel covers 5.71 x 5.71 mm. The design focus point of the beam down configuration is the center of the 4m x 4m square.

Weighted Flux Map

For the upcoming analysis we will assume a receiver with two concentric circular apertures as shown in Figure 3. The inner region is where most of the energy and the highest concentration are expected; physically this can be the aperture of the main high temperature receiver, the radius of this aperture is r_1. Some of the concentrated radiation will reach the region between the two circles ($r_1<r<r_2$), generally this radiation will have less concentration and less energy than the inner region, thus it can be used for pre-heating the HTF before entering the inner receiver. According to the previous argument, for each point in the matrix a weighted value can be calculated by the following formula:

$$Q(x,y) = \begin{cases} 1\,, r \le r_1 \\ G * \left(\frac{r_2 - r}{r_2 - r_1}\right)\,, r_1 < r < r_2 \\ 0\,, r \ge r_2 \end{cases} \quad Eq(1)$$

In Equation (1) the flux intensity *G*, the flux intensity is multiplied by 1 in the inner region, in the outer region the flux points are multiplied by zero meaning that energy in that region is not useful, while the flux map is linearly weighted in the region in between the two apertures, over all the weighting function will be trapezoidal, see Figure 3.

The flux map produce by the CCD camera contain luminance (cd/m^2) values; these values are assumed to be a measure of flux intensity *G*. To convert luminance values into heat flux units a constant conversion factor is assumed (this constant might be varying throughout the test reference to the other paper). *G* is then normalized by the DNI at the time of the measurement, DNI records are available from the weather station every ten minutes thus interpolation was required to get DNI values at the step times of the test.

Before we can use equation (1), the centroid of the flux map should be calculated, and the receiver dimensions (r_1 and r_2) should be selected.

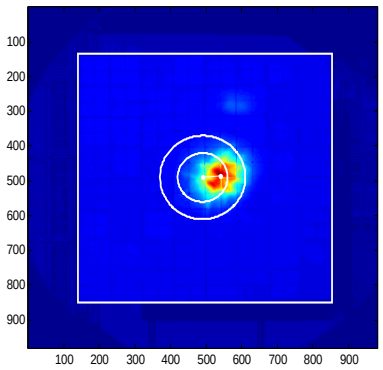

Figure 3 Typical flux density map generated by the overhead CCD camera (Resolution: 980x980 pixels).

Centroid and Offset Calculation

The first step in analyzing the flux map is to find the flux map centroid. This could be easily done by finding the x and y coordinates of the centroid Cx, Cy respectively:

$$C_x = \frac{\sum G(x,y) * x}{\sum G(x,y)} \;\; and \;\; C_y = \frac{\sum G(x,y) * y}{\sum G(x,y)} \quad Eq(2)$$

Applying this equation on the raw flux map will result in unwanted results as the calculation will be affected by the ambient radiation falling on the receiver (since we are dealing with low concentration of only one heliostat at a time) thus some filtering of the flux map is necessary in order to calculate the centroid coordinates.

The points of the flux map which should be filtered are those of ambient radiation on the plane of the receiver. These will generally correspond to the lowest points in the flux map unless there is a shadow on the receiver casted by the secondary reflector or one of its three pillars. Thus the filtered flux map is given by equation 3 below, where $g_{ambinet}$ is the ambient radiation, k is the filter parameter, G(x,y) is the original flux map, G'(x,y) is the filtered flux map :

$$G'(x,y) = \begin{cases} G(x,y) - k * g_{ambient}, & G(x,y) - k * g_{ambient} > 0 \\ 0 \quad , & G(x,y) - k * g_{ambient} \le 0 \end{cases} \quad Eq(3)$$

- **Finding $g_{ambient}$:**

$g_{ambient}$ is found using the Matlab™ function (mode) which gives the most frequent value (MFV) in the flux map. MFV will most probably correspond to a point outside the region of heliostat radiation, and thus will correspond to ambient radiation (eg. See Figure 3).
Shadows make the detection of the value of $g_{ambient}$ a bit more complicated, since the lowest value of the flux map doesn't correspond to ambient radiation anymore, thus instead of finding MFV of the whole flux map, we find it for each of the four corners of the flux map; these areas don't normally have any radiation from the heliostat, and at most 3 corners could be shaded at a time, thus $g_{ambient}$ will most probably correspond to the maximum of the 4 MFVs that we found for each corner. We also increase the odds of finding $g_{ambient}$ by rounding the matrix values to the nearest integer and thus increasing the number of pixels having similar values.

- **Filtering for Centroid Calculation:**

To calculate the centroid correctly we need to get rid of ambient radiation points from the flux map using equation 3, ideally we should only remove ambient radiation points thus setting k to 1 in equation 3, however some scattered radiation coming from the heliostat may also affect the calculation, thus we use a value slightly greater than 1, k=1.2 was found to give good centroid detection

- **Filtering for calculating cumulative power curve :**

In order to calculate the curve in Figure 5, we should make sure the energy in the flux map is only from the heliostat and does not include any ambient radiation (GHI). Thus we use a value of k=1 for this purpose.
After calculating the centroid the offset (distance between the geometrical center and the flux map centroid) can be easily calculated to measure the error in the flux map position resulting from misalignment in the heliostats, in the tracking photo-sensor, or in the corresponding secondary reflector mirror.

Selecting receiver dimensions

In order to dimension the hypothetical receiver that we are going to use in the analysis we selected four of the best flux maps and we base the receiver dimensions on these four maps. In Figure 4 the mean radiation at a given radial distance from the flux map centroid is plotted as a ratio of the theoretical maximum or upper limit for possible radiation, this limit is based on the concentration factor of the heliostat, the heliostats used in the beam down have 42 flat facets which are canted to one imaginary focus point at the focal point of the secondary reflector. Thus the upper limit for the power indicated by one of the pixels in the flux map will be (DNI*NumberofHeliostatFacets*PixelArea). From the figure it can be seen that the power drops to lower than 3% of the theoretical maximum for radial distance greater than 100 pixels or 0.571m, moreover, it can also be seen that none of the flux maps exceeds 25% of the theoretical maximum.

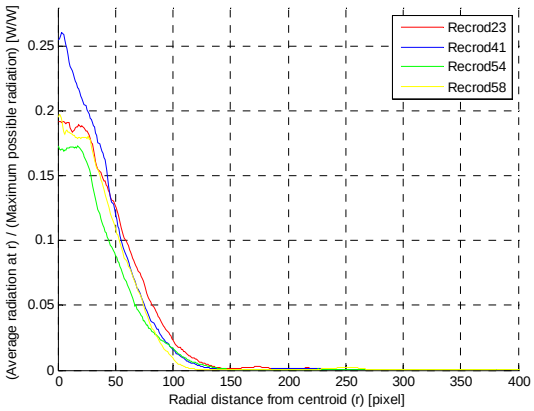

Figure 4 Mean radiation at a radial distance (r) from the centroid of the flux map, normalized by the theoretical maximum power given by (DNI*number of flat heliostat facets*area of one pixel), this theoretical maximum is the upper limit of radiation concentration as it clearly ignores cosine factor, incidence angle, reflectivity of the mirrors in addition to other things.

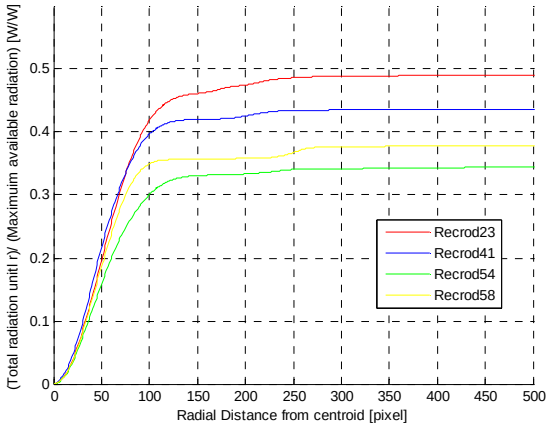

Figure 5 Cumulative power intercepted by the receiver from the centroid until the radial distance (r), normalized by the maximum theoretical total power (DNI * Heliostat Area). This theoretical maximum is the upper limit of radiation concentration as it clearly ignores cosine factor, incidence angle, and reflectivity of the mirrors in addition to other things.

Figure 5 depict the flux map in cumulative form; total power included in the circular region of radius (r) around the centroid is normalized by the maximum power that can be reflected to the receiver, (DNI*Heliostat Area).

Figure 5 has a significant value in comparing heliostat performance, not only is it a measure of the amount of energy that the heliostat is reflecting to the receiver compared to what is available, but also it indicates how well the heliostat is concentrating the reflected energy, for example if we take a look at Record23, it is clear that the it is the best heliostat that approaches it theoretical limit (eventually up to 56%), moreover it achieves a more than 42% within a radial distance of 100 pixels, compared to Record 41 which achieves the same ratio at 112 pixels.

We can notice some crossing-over between the curves (e.g. Records 54&58 and 23&42) and this means that the quality of each flux map depends on the chosen radii of the receiver. Choosing a receiver radius under 50 pixels will favor Record41 over 23, however if the receiver radius was above 75 Record 23 will be favored.

By studying Figure 4 and Figure 5, we have chosen values of r1=70 and r2=120. This way we can make use of the highly concentrated radiation in the inner receiver and still make of use a considerable amount of the energy by having the second receiver (e.g. CPC) at r2.

Figure 6 is similar to Figure 5 but with the x axis scaled to better show the region of interest. The curves are normalized by the actual total power instead by the theoretical total power. Actual power is the total power reflected from the heliostat to the target (thus, ambient radiation is excluded), this is calculated using Equation (3) setting k to 1 and then integrating the flux map over the target area.

$$P_{target} = \int G'(x,y)dA \qquad Eq(4)$$

We can see from the figure that by choosing a radius r_1=70, for all the shown records more than 60% of the total power will be intercepted in the inner receiver, and that more than 90% of the power will be intercepted by the whole receiver. Figure 7 depicts the corresponding flux maps with the receiver apertures.

We assume that the designers have aimed for a certain flux distribution (concentration and optical efficiency) knowing that there is some uncertainty in achieving the said target. Now faced with the real flux distribution one can design a receiver optimized for a given (range of) operating temperature. Since receiver design is not the subject of this paper, we aim to intercept some fraction of the reflected power incident on the whole target.

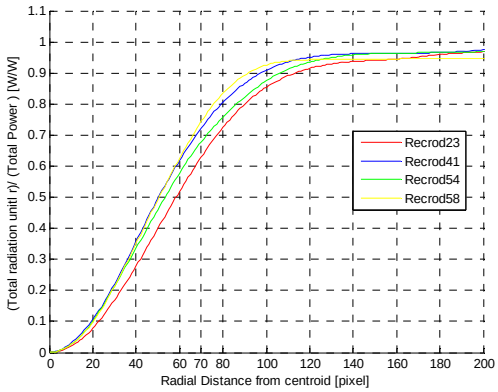

Figure 6 Cumulative power intercepted by the receiver from the centroid until the radial distance (r), normalized by the total power.

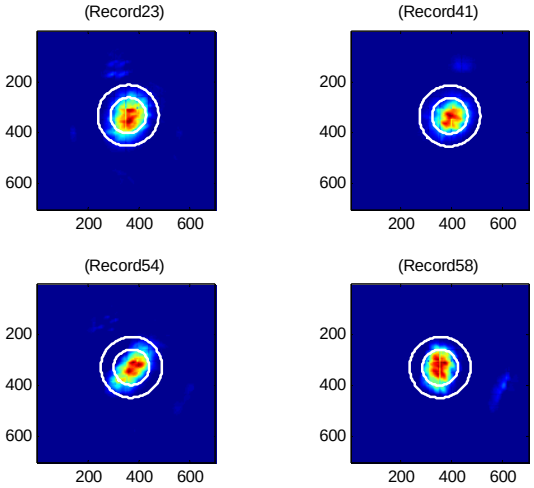

Figure 7 Flux maps with receiver apertures drawn around the centroid, flux maps where filtered using equation 3 and a k value of 1.

IV. Results

One of the aims of this test is to assess the performance of the individual heliostats in each of the three fields (sectors), and to compare it to the performance of other heliostats. One sector is tested each day for five time steps which are chosen throughout the day (the middle time step being at solar noon). At each time step all heliostats of that sector are tested.

Data were collected for 6 days (twice for each field) in March. March represents one of the best months of the year in terms of DNI because summer haze and dust are frequent in Abu Dhabi. Unfortunately we had to discard the data of one of the test days of the east field because of reliability issues. In addition we will only present a summary of the results due to space limitation.

Three performance parameters are chosen to interpret the data collected. First is the amount of power intercepted by the receiver aperture (weighted using equation (1)) normalized by the DNI at time of measurement, this parameter is a measure of the overall optical performance of the heliostat and how will it concentrates the radiation inside the aperture, since the calculation is based around the centroid of the flux map and not on the center of the receiver, this parameter does not include centering.

Table 1 Intercepted power normalized by incident DNI

	North18	North20	East22	West27	West29
Average	24.0%	25.1%	21.8%	15.8%	25.1%
Standard Deviation	10.2%	9.5%	9.1%	7.1%	9.3%
Minimum	0.5%	1.2%	7.5%	2.4%	4.4%
Maximum	43.2%	40.9%	64.4%	30.4%	44.8%

Table 1 summarizes the statistics of the this parameter for the data set, it can be seen that the average values range from around 15.8% up to 25.1%, generally the maximum percentage of intercepted DNI lies around 45% for most of the cases, but for some heliostats it can reach values as high as 64.4% as in East22.

A better representation of concentration quality of a certain heliostat can be obtained by the ratio of the intercepted power and the total power reflected on the target (the later given by equation (4)), or as is commonly referred to as the intercept factor. Table 2 summarizes the results of the intercept factors of our hypothetical receiver. Generally the receiver intercept factors are high, by design, average values are around 75% while maximum values can reach more than 97%.

Table 2 Intercept Factor

	North18	North20	East22	West27	West29
Average	76.4%	76.0%	72.1%	74.4%	73.5%
Standard Deviation	11.2%	11.2%	10.7%	13.7%	13.8%
Minimum	48.3%	47.0%	40.1%	28.0%	37.0%
Maximum	97.0%	97.2%	95.3%	95.3%	95.0%

Centering is measured by the offset, which is the distance between the calculated flux map centroid and the geometrical center of the receiver. Deviation from the ideal value of zero is most probably due to misalignment in the tracking sensor or in the secondary reflector mirror corresponding to the heliostat in question. Compared to other errors, offset can be easily fixed, that is why it values for offset are reported separately, Table 3. Values around 40 are typical as can be seen from the table, maximum values are quiet far however, but this might be a bit misleading as error in calculating the centroid will dramatically affect the offset calculation, this is probable when dealing with "bad" heliostats in which the power levels are low or when aberrations are high.

Table 3 Flux map offset

Field-Day	North18	North20	East22	West27	West29
Average	40.0	37.6	39.9	44.3	44.1
Standard Deviation	22.9	18.7	22.9	19.4	16.0
Minimum	1.8	3.0	1.8	5.0	8.8
Maximum	139.0	108.3	138.8	127.0	103.4

V. Discussion and Observations

One of the important aspects of this test is the ability spot irregularities in the heliostat field and/or to get better understanding of the heliostat field and some complex aspects of blocking and shading especially for such an unusual optical design of both the tower and the heliostats.

Shading

As it is hard to inspect each and every flux map in detail, the previously discussed parameters can lead us to the discovery of some issues which are hard to detect manually, when suspicious values are detected. For example heliostats A3 and A4 (North sector) at noon time-step had very low ration of intercepted power to incident DNI, looking at the corresponding flux maps in Figure 8 .We can see that there is only ambient flux on the receiver in addition to the shadow casted by one of the three pillars of the central reflector. The two heliostats were completely shadowed by the central reflector for the entire noon period. This problem could have been avoided by moving the heliostats in the North sector farther from the tower.

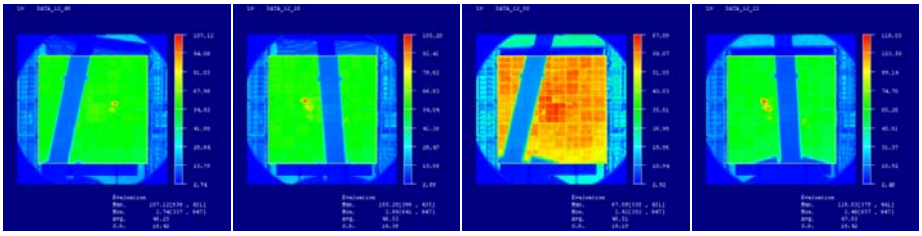

Figure 8 Complete shading of "A-line" heliostats in the North sector

Heliostat concentration Errors

There are some undesirable patterns which were spotted by looking at the flux maps and the performance parameters. These patterns seem to happen at high azimuth angles and angles of incidence in general and thus are probably a result of off-axis aberration. Other possible causes of these patterns are the canting errors of the heliostat mirrors and deformed central reflector mirrors. The flux maps below show some examples.

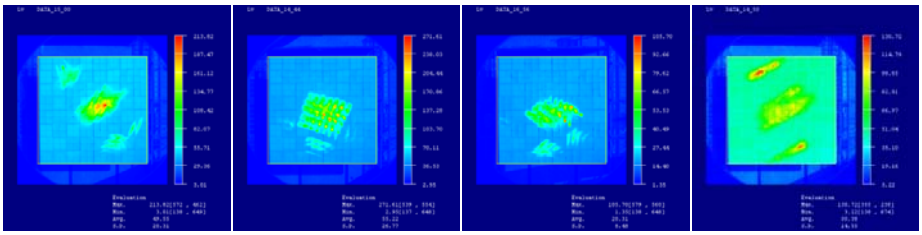

Figure 9 Heliostat concentration errors

References

[1] Francisco J. Collado and Jesús Guallar, "Design of Solar Tower Plants Heliostat By Heliostat: The Blocking Factor," *SolarPaces*, 2009.

[2] Marcelino Sa´nchez and Manuel Romero, "Methodology for generation of heliostat field layout in central receiver systems based on yearly normalized energy surfaces," *Solar Energy*.

[3] Hiroshi Hasuike et al, "Demonstration of Tokyo Tech Beam-Down Solar Concentration Power System in 100kW Pilot Plant," *SolarPaces*, Germany: 2009.